Axisymmetric Shell Analysis of the Space Shuttle Solid Rocket Booster Field Joint

Michael P. Nemeth*
NASA Langley Research Center, Hampton, Virginia
and
Melvin S. Anderson†
Old Dominion University, Norfolk, Virginia

The Space Shuttle Challenger (STS 51-L) accident led to an intense investigation of the structural behavior of the solid rocket booster (SRB) tang and clevis field joints. The presence of structural deformations between the clevis inner leg and the tang, which were substantial enough to prevent the O-ring seals from eliminating hot gas flow through the joints, has emerged as a likely cause of the vehicle failure. This paper presents results of axisymmetric shell analyses that parametrically assess the structural behavior of SRB field joints subjected to quasi-steady-state internal pressure loading for both the original joint flown on mission STS 51-L and the redesigned joint recently flown on the Space Shuttle Discovery. Axisymmetric shell modeling issues and details are discussed and a generic method for simulating contact between adjacent shells of revolution is described. Results are presented that identify the performance trends of the joints for a wide range of joint parameters.

Nomenclature

d, d^*	= radial distance between tang and clevis inner leg prior to and after motor pressurization
F_j	= contact forces, $j = 1 \rightarrow 7$ (Fig. 10)
G_j	= radial distance between shell wall surfaces corresponding to F_j, $j = 1 \rightarrow 7$ [Eq. (A1)]
H_0,H_1	= dimensions of tang and clevis pin region model (Fig. 2)
N	= number of contact points (Appendix)
P	= pressure due to burning of solid propellant
t_1,t_2	= dimensions of capture feature and clevis inner leg (Fig. 3b)
Δ	= O-ring gap change defined by $\Delta = d^* - d$
Δ_{ri}	= radial displacement at point r due to influence loads associated with F_i (Fig. 10)
Δ_{rp}	= radial displacement at point r due to pressure loading (Fig. 10)
$\delta_1, \ldots, \delta_5$	= initial joint clearances (Fig. 3)
μ	= joint clearance defined by $\mu = t_2 - t_1 = \delta_4 + \delta_5$ (Fig. 3b)

Introduction

An intense effort has been underway at the NASA Langley Research Center to study the structural behavior of the right solid rocket booster (SRB) since the loss of the Space Shuttle Challenger (STS 51-L). Review of the evidence and facts leading up to the loss of the vehicle has focused on failure of the aft tang and clevis field joint of the right SRB as the probable cause of the accident.[1] Structural analyses of this field joint have been performed on several levels at the Langley Research Center and the Marshall Space Flight Center. These levels range from simple axisymmetric shell analyses to very sophisticated three-dimensional inelastic finite-element analyses. The axisymmetric shell analyses were used to identify the qualitative joint behavior trends and to provide guidance for the more sophisticated analyses. This paper focuses on elastic axisymmetric shell analyses performed using the computer program FASOR.[2] Specifically, the paper describes modeling issues necessary to adequately predict the qualitative joint behavior trends, and presents a generic methodology for parametrically simulating contact within the joint as a function of the initial joint clearances. The method presented herein allows very rapid calculation of joint response so that parametric studies involving a large number of parameters are practical. Some results of parametric studies showing joint behavior trends as a function of initial clearances are presented for the original and redesigned SRB field joints. The results indicate that the redesigned joint provides a substantial improvement in the performance of the SRB field joint over the original joint design.

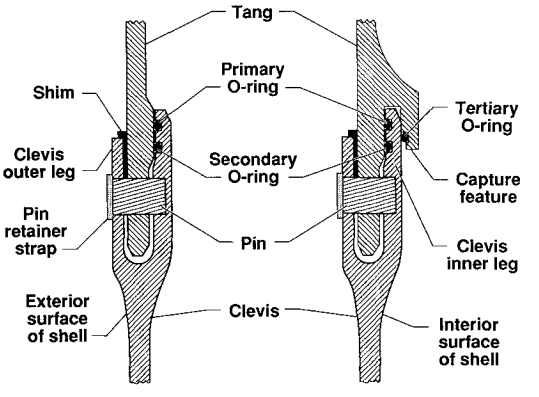

Fig. 1 Original and redesigned field joint cross sections.

Received Feb. 24, 1989; presented as Paper 89-1343 at the AIAA/ASME/ASCE/AHS 30th Structures, Structural Dynamics, and Materials Conference, Mobile, AL, April 3-5, 1989; revision received May 23, 1989. Copyright © 1989 American Institute of Aeronautics and Astronautics, Inc. No copyright is asserted in the United States under Title 17, U.S. Code. The U.S. Government has a royalty-free license to exercise all rights under the copyright claimed herein for Governmental purposes. All other rights are reserved by the copyright owner.

*Research Engineer, Structural Mechanics Branch, Structural Mechanics Division.

†Research Professor, Mechanical Engineering and Mechanics Department, Associate Fellow AIAA.

Problem Overview

The original and redesigned SRB field joints shown in Fig. 1 consist of a male-to-female pin-connected joint between two cylindrical shells, referred to as solid rocket motor (SRM) cases, which are approximately 3.7 m (12 ft) in diameter and 9.1 m (30 ft) long. The male and female parts of the joint are referred to as the tang and clevis, respectively. The parts of the clevis on the inside and outside of the cylinder are referred to as the inner and outer legs, respectively. The original joint uses two O-rings to provide a pressure seal between two SRM cases. The redesigned joint has an additional part on the tang, referred to as the capture feature, which is intended to limit the deflections between the tang and clevis inner leg. The redesigned joint is based on the original joint design concept with small differences in dimensions, the addition of the capture feature, and the presence of a third O-ring.

A total of 180 pins spaced equally around the joint circumference are inserted into holes that are machined through the tang and partially through the clevis, for both the original and the redesigned joints, as indicated in Fig. 1. The pins are held in place by a metal retainer strap on the outer surface of the joint. Metal shims are placed between the tang and clevis outer leg to reduce the initial joint clearance between the tang and inner clevis leg. Rubber O-rings are used to provide a pressure seal during motor operation. The effectiveness of the O-rings in providing this seal depends on the relative displacements of the parts of the joint in the proximity of the O-rings.[1]

The Space Shuttle experiences a number of dynamic loading conditions prior to and during the 2-min-long part of the ascent when the SRBs are operational. An important loading condition for the boosters that is addressed herein is the maximum quasi-steady-state internal pressure of approximately 6.895 MPa (1000 psi) exerted on the shell wall by solid propellant burning during vehicle ascent.

Modeling Assumptions and Details

Two SRM cases joined together by either the original or redesigned field joint possess periodic circumferential symmetry. A basic repetitive meridional element of the joined SRM cases that possesses the same stiffness, loading, and support conditions when translated circumferentially by a finite angle can be identified. For the SRM cases, this angle is 2 deg. Since this angle is relatively small, it is assumed that the overall stiffness of the field joint can be matched closely enough by axisymmetric analysis to adequately represent the structural behavior of the joint in the vicinity of the O-ring pressure seals. The SRM field joint has several modeling issues that must be addressed when using an axisymmetric shell analysis, especially when local joint behavior trends are the desired end result of the analysis. The issues that appear to be most important are the modeling of the pin connection, the local stiffness reduction associated with the pin hole and O-ring grooves, the internal pressure distribution near the O-rings, the way in which the load is transferred between the tang and clevis by the pin reaction forces, and the clearances between the tang, clevis, and pin. The joined SRM cases are fabricated using D6AC steel and the nominal material properties for this material used in the analyses are $E = 200$ GPa (29×10^6 psi) for Young's modulus and $\nu = 0.3$ for Poisson's ratio.

Local Stiffness Modeling Details

The tang is connected to the clevis by discrete pins that can only be modeled by continuous shell segments in a shell of revolution analysis. To simulate the actual three-dimensional flexibility of the joint as accurately as shell analysis will permit, the shell segments representing the pin are assumed to only contribute meridional stiffness to the joint model. This assumption is implemented in the FASOR model by eliminating the circumferential stiffnesses of the shell segments representing the pin connection. The meridional extensional and bending stiffnesses of the shell segments representing the pin are approximated by EA/s and EI/s, where s is the pin spacing and EA and EI are the extensional and bending stiffnesses of a pin, respectively.

The circumferential variation in stiffness of the shell due to the pin holes is approximated by using a reduced value of stiffness that is assumed to be constant around the circumference of the shell, which is consistent with shell of revolution analysis. The stiffness reduction associated with the pin holes is implemented in the FASOR model by introducing a linear thickness variation over the pin hole region for the tang and both clevis legs. This region of thickness variation for the original joint and a typical element of the tang or clevis legs are shown in Figs. 2a and 2b, respectively. The linear thickness variation used in the FASOR models is determined by requiring the models to have an average meridional bending stiffness that matches stiffnesses determined in unpublished plate bending experiments performed in the Structures Laboratory at NASA Langley Research Center. These experiments consisted of four-point bending tests of flat plates with holes approximately 2.54 cm (1.0 in.) in diameter and with hole spacings identical to that of the SRM case field joint, and are intended to represent the actual flight hardware within the fidelity of the shell model. Plate thicknesses used in the experiments were those of stock items that were close to the thicknesses of the actual tang and clevis legs. Holes were drilled completely through the plates used to simulate the tang and clevis outer leg, and drilled partially through (to the corresponding depth of the holes in the clevis inner leg) the plate intended to simulate the clevis inner leg. The experimental results indicate bending stiffness reductions due to holes in the clevis outer leg and tang, and due to holes drilled partially through the clevis inner leg at approximately 57, 63, and 58% of the bending stiffnesses of the corresponding plates without holes. The dimensions H_0 and H_1 of the linear thickness variations used in the FASOR model of the pin region depicted in Fig. 2b are determined by analytically finding the thickness H_1 that produces the same bending stiffness reductions that were obtained in the experiments. The dimension H_0 is predetermined by the dimensions of the tang and clevis legs.

A reduced meridional stiffness of the clevis inner leg is implemented in the FASOR model to account for the fact that the O-ring grooves cannot have meridional stresses acting on their traction-free surfaces. The region where the stiffnesses are modified is assumed to cover the shaded region shown in Fig. 2c. The FASOR program allows the input of orthotropic elastic moduli, and this convenience is used to selectively modify the stiffnesses of the O-ring grooves. The shaded region between the O-ring grooves is assigned a zero value of elastic modulus in its meridional direction. The meridional stiffness in the remaining shaded regions shown in Fig. 2c are calculated using an elastic modulus in their meridional direction that varies from the full value to zero at the traction-free surfaces of the O-ring grooves. For all of the shaded regions shown in Fig. 2c, the full circumferential stiffness is retained.

Local Pressure Distribution Modeling Details

The relative displacements between the tang and clevis inner leg in the vicinity of the O-rings is dependent on where the pressure seal actually occurs. Three pressure seal cases are considered in the analysis of the original joint. The first case corresponds to one in which the pressure has been prevented from reaching the O-ring seals altogether by the SRM internal insulation. This case corresponds to the factory assembly of two SRM cases in which a rubber liner totally seals the joint (referred to as a factory joint) and the pressure never reaches the O-rings. The second and third pressure seal cases are defined by the instances in which the primary and secondary O-rings independently seal the joint, respectively.

As previously mentioned, the redesigned joint contains an additional O-ring, referred to herein as the tertiary O-ring. The pressure distributions investigated in the analysis of the redesigned joint correspond to the cases in which the tertiary,

primary, and secondary O-rings seal the joint independently. For all of these cases, when the pressure acts on both surfaces of a shell segment (as may occur on the clevis inner leg shown in Fig. 1), the net result is negligible within the limits of thin shell theory.

Pin-Tang-Clevis Load Transfer Modeling

The nominal 6.895 MPa (1000 psi) internal pressure generated by propellant burning induces an axial load in the shell wall of 63,650 N/cm (36,345 lb/in.) corresponding to the biaxial state of stress occurring in a sealed pressure vessel. This axial load corresponds to approximately 413,350 N (92,220 lb) of axial force that is transferred by each pin. The load transfer between the tang, clevis, and pins occurs in a periodic manner. Moreover, the pins bear on the tang and clevis to produce a contact stress distribution within each pin hole. The way in which the pins bear on the clevis inner leg, through the thickness of the shell, generally depends on the amount of pin deformation, the clearances in the pin hole, the amount of beveling of the edges of the pin, friction between the pin and the tang and clevis, and any inelastic deformations that result from high stresses. Associated with the contact stress distribution of a pin is a resultant pin reaction force. The large size and the proximity of the pin reactions to the O-ring pressure seals suggest that the manner in which the pins bear on the clevis inner leg is an important modeling detail to be addressed.

Axisymmetric shell analysis cannot capture the local nature of the periodic pin contact stresses, but can simulate the actual load transfer with a statically equivalent uniform load distribution. This simulation is accomplished by investigating the sensitivity of the FASOR model to the location of the reference surface of the clevis inner leg. The length of the shell segment connecting the clevis inner leg to the tang depends on the location of the shell wall reference surface. Varying the length of this connecting shell segment changes its bending stiffness and indirectly changes the location of the resultant pin reaction force.

As previously discussed, the stiffnesses of the shell segments representing the pin are modified to include only meridional stiffness since the pin contributes essentially no circumferential stiffness to the joint. Joining the tang and clevis in this manner constrains the tang from sliding on the pin and corresponds to a no-slip connection between the tang, clevis, and pin. Preventing slippage between the tang, clevis, and pin was shown to be an important modeling issue of the SRM joint.[3]

Clearances and Contact Modeling

The results of the "referee tests" of the original SRM field joint performed at Morton-Thiokol, Inc.[4] have indicated an effect of initial clearances on the relative displacements between the tang and clevis inner leg at the O-rings. Ideally, it is desirable to know the effect of a wide range of clearances on the structural behavior of the field joint. This effect is studied by applying an influence coefficient method in which pairs of loads are applied to assumed contact points on adjacent shell walls. This influence coefficient method, however, does not address clearances and contact between the pin, tang, and clevis legs. The locations and number of contact points required to sufficiently simulate the joint behavior were determined in the present study by examining the joint deflections obtained from shell analyses of the joint in which adjacent shell walls were free to overrun one another. This effort led to the selection of points on adjacent shell walls corresponding to locations A, B, and C of the original joint shown, in Fig. 3a, and to locations A–G of the redesigned joint shown in Fig. 3b, as the contact locations. Associated with each contact point is an initial clearance indicated by δ_1–δ_5 in Fig. 3. These clearances represent the radial distance between adjacent shell walls prior to assembly and pressurization of the joint. The clearance δ_1 is particularly significant in that it corresponds to the shimming process applied to the joint during assembly. The range of values of δ_1 investigated in this study includes all shim sizes used in the "referee tests" and on the actual flight articles. Thus, the maximum value of δ_1 corresponds to a joint without shims, and a zero value corresponds to a joint where the shimming process produces a perfect contact between the adjacent shell walls resulting in no clearance.

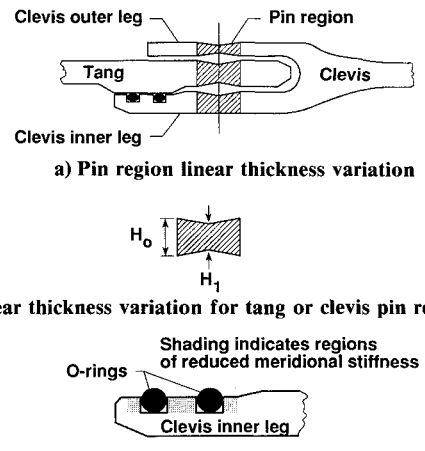

a) Pin region linear thickness variation

b) Linear thickness variation for tang or clevis pin region

c) O-ring groove details

Fig. 2 Pin hole and O-ring groove modeling details.

The basic idea behind the contact analysis is to compute the forces at two assumed contact points that are necessary to prevent adjacent shell walls from overlapping. This task is accomplished by enforcing radial displacement compatibility between two assumed contact points when the deflections and clearances are such that contact occurs. The relative displacements between the tang and clevis at the O-rings are then adjusted to reflect the presence of any contact forces. For a given set of clearances and N possible contact locations, there exist 2^N possible contact conditions that can be determined by analysis. There is, however, only one physically admissible solution. This solution is found by excluding all solutions that produce tensile contact forces and inadmissible relative displacements (overrun) between adjacent shell walls. An algorithm was developed to determine the physically admissible solution. Details of the algorithm are given in the Appendix.

Results and Discussion

The effectiveness of the O-rings in providing a pressure seal inside the solid rocket boosters to eliminate hot gas flow through the SRM field joints depends heavily on the relative radial displacements between the tang and clevis inner leg in the proximity of the O-rings. A specific relative displacement is used in this paper to assess the joint performance and represents the joint displacement that an O-ring must follow during motor pressurization to insure safe operation. This important parameter, for both the original and redesigned joint, is the relative radial displacement between the inner surface of the tang and the outer surface of the clevis inner leg midway between the primary and secondary O-rings. After joint assembly, the radial distance (referred to herein as gap) separating adjacent surfaces of the tang and clevis inner leg, between the primary and secondary O-rings, is a specific amount denoted as d. After motor pressurization, the gap d between adjacent surfaces of the tang and clevis inner leg changes to a different gap d^*. The relative radial displacement that the O-rings must follow to insure a pressure seal is given by $\Delta = d^* - d$, and is referred to hereafter as the O-ring gap change. Positive values of Δ represent further separation of the tang and clevis inner leg, whereas negative values indicate the tang and clevis inner leg are closer together after motor pressurization.

Results for the Original Joint

The linear FASOR analysis of the original SRM joint yielded O-ring gap changes ranging from 0.053–0.066 cm

(0.021–0.026 in.). This range of displacements was obtained for values of clearances δ_1 and δ_2 ranging from 0–0.127 cm (0.050 in.) and a nominal value of δ_3 equal to 0.127 cm (0.050 in.) (see Fig. 3a). Similar results obtained using three-dimensional finite-element analysis are presented in Refs. 3, 5, and 6, and these results indicate O-ring gap changes ranging from approximately 0.048–0.094 cm (0.019–0.037 in.). The variation in the O-ring gap changes reported in Refs. 3, 5, and 6 was attributed to differences in local modeling details and clearances around the pin and pin-hole region, and clearances between the tang and clevis. The lower value of O-ring gap change corresponds to the ideal case of a joint with a perfectly fitting pin and zero initial clearances.

As discussed previously, axisymmetric shell analysis cannot simulate the local details of the pin region such as clearances and pin-edge bevel exactly, and thus the analysis treats the pin connection as an ideal connection. One modeling parameter that can be adjusted in the shell analysis is the location of the reference surface of the clevis inner leg. This parameter determines the length of the shell segment connecting the clevis inner leg to the tang and, hence, affects its bending stiffness and indirectly determines the location at which the statically equivalent pin reaction force is transferred to the clevis inner leg. Results obtained for several different reference surface locations indicate that moving the reference surface from the innermost side of the clevis inner leg toward the tang results in only minor differences in the O-ring gap change computed and a slight reduction in the sensitivity of the displacements to the initial clearances δ_1 and δ_2. The largest variation in O-ring gap changes, associated with varying the initial clearances, ranges from 0.041–0.058 cm (0.016–0.023 in.) and corresponds to a reference surface located at the inner surface of the clevis inner leg. Because of the fairly benign influence of reference surface location on the O-ring gap changes, a single reference surface location was used to perform the remaining parametric studies. This reference surface location is approximately at the midpoint of the slot in the clevis inner leg that the pin fits into [0.8090 cm (0.3185 in.) outboard from the interior surface of the clevis inner leg]. In addition, the effect of varying the initial clearance δ_3 on the O-ring gap change was found to be benign and was eliminated as a parameter in the study of the original joint.

The O-ring gap changes recorded in the referee tests performed by Morton-Thiokol[4] ranged from 0.051–0.104 cm (0.020–0.041 in.), depending on circumferential location around the joint and the size of the shims used (see Fig. 1). The gap changes recorded were obtained from a pressure loading approximately 1% higher than the 6.895 MPa (1000 psi) pressure loading used in the analysis presented herein and in Refs. 3 and 5. The results of Ref. 6 correspond to the same value of pressure as that used in the referee tests, namely 6.923 MPa (1004 psi). The presence of a substantial variation in joint and pin clearances around the circumference of the shell was noted in the experiment. Specifically, measurements made on the tang and clevis prior to testing indicated that clearances between the tang and both clevis legs, in the proximity of the O-rings, could vary from 0.089–0.165 cm (0.035–0.065 in.) around the circumference of the shell. These clearances correspond to values of δ_1 ranging from 0 to approximately 0.076 cm (0.030 in.), for the shim sizes used in the referee tests.

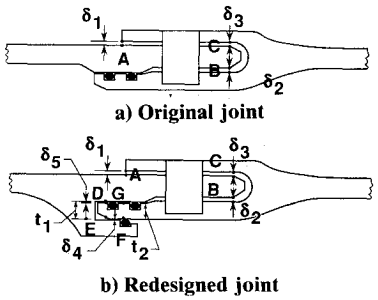

a) Original joint

b) Redesigned joint

Fig. 3 Clearances and contact points for original and redesigned joints.

The results of the FASOR analyses, the three-dimensional finite-element analyses, and the referee tests are presented in Fig. 4. The distribution of results shown for the FASOR analyses corresponds to O-ring gap changes obtained by varying the clearances δ_1 and δ_2 from 0–0.127 cm (0.050 in.). The distribution of results shown for the three-dimensional finite-element analyses ranges from displacements corresponding to an ideal joint with zero clearances to larger displacements corresponding to additional flexibility associated with the pin, pin-edge bevel, and initial clearances (including clearances around the pin). The results shown for the referee tests were affected by small amounts of local plasticity in the vicinity of the pin connections in addition to joint clearances and exhibited a slight nonlinear behavior according to Ref. 4. The FASOR analyses indicated stresses in excess of the yield stress also in the pin-connection region of the shell-of-revolution model. However, since the areas of plasticity indicated by the shell-of-revolution analyses were in the relatively small region of the joint where thicknesses were tapered to simulate the reduced bending stiffness of the pin holes, it was considered unrealistic to include plasticity in the axisymmetric analyses since the actual area of plastic deformation was in the localized pin bearing area.

The results of Fig. 4 show that both the FASOR analyses and the three-dimensional finite-element analyses yield O-ring gap changes that are in the range of the experimental results. Moreover, the results of the FASOR analysis and the three-dimensional finite element analysis are in good agreement when the joint is assumed to be free of initial clearances (ideal joint). The maximum O-ring gap changes corresponding to three-dimensional finite element analysis and "referee tests" show good agreement and indicate that the local pin clearances, pin-edge bevel, and pin deformations are important to predict the structural deformations precisely. However, the reasonably good qualitative agreement between the results of the FASOR analyses and the three-dimensional finite-element and experimental results, and the relative simplicity of the FASOR analysis, suggests that the axisymmetric shell analysis presented herein is useful for identifying structural trends of the SRM joints for a large range of parameters in a timely and relatively inexpensive manner.

Results obtained from FASOR analyses and from the "referee tests" showing the sensitivity of the O-ring gap changes to local pressure distribution near the O-rings and initial clearances are presented in Fig. 5. The parameter x shown in this figure is the distance measured from the tip of the clevis inner leg toward the pin, and indicates the point at which the pressure distribution changes from being applied to the tang to being applied to the clevis inner leg. The band of results in Fig. 5 obtained from the FASOR analyses corresponds to clearances ranging from $\delta_1 = \delta_2 = 0$ to 0.127 cm (0.050 in.) and includes results for all clearances between these bounding values. These results indicate that preventing the pressure from reaching the O-rings (like the factory joints) produces the smallest O-ring gap changes for the full range of joint clearances. As the parameter x increases to values that correspond to the locations of the centers of the primary and secondary O-rings, the band of displacements increases to between 0.051–0.064 cm (0.020–0.025 in.) and between 0.076–0.091 cm (0.030–0.036 in.), respectively. The referee tests results indicate the same trend as the FASOR results, but with somewhat larger O-ring gap changes and data scatter due to the added flexibility associated with the variation in clearances, plasticity, slight geometric nonlinearity, and slightly higher operating pressure.

The nonlinear static response of the joint was also determined as a function of the initial joint clearances. The nonlinear contact solutions were obtained by applying the incremental procedure described at the end of the Appendix. This procedure converges rapidly indicating a very slight, and es-

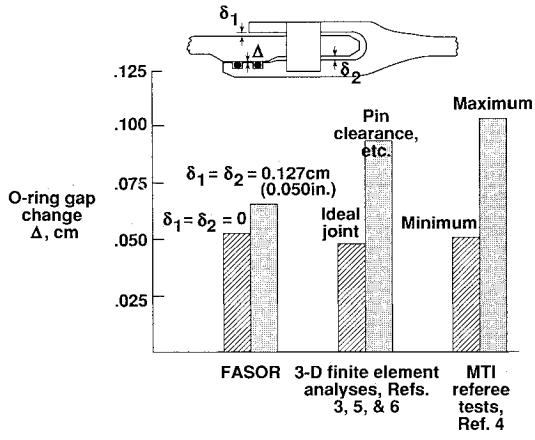

Fig. 4 Comparison of O-ring gap changes obtained from two-dimensional and three-dimensional analyses with experimental results for original joint.

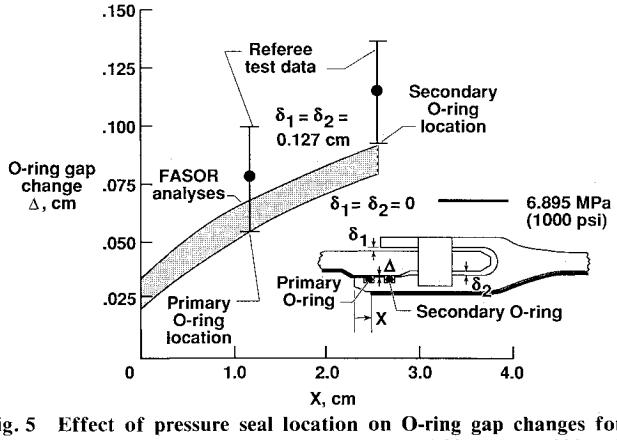

Fig. 5 Effect of pressure seal location on O-ring gap changes for original joint [bold line denotes regions where 6.895 MPa (1000 psi) normal pressure acts].

sentially benign, influence of geometric nonlinearity on the O-ring gap changes. Because of the benign influence of geometric nonlinearity obtained in the FASOR analyses and reported in the referee tests, the remaining analyses presented herein neglect geometric nonlinearity.

Results for the Redesigned Joint

The results presented in Figs. 6 and 7 show the effects of initial clearances on the O-ring gap changes for the redesigned joint. In particular, the results presented in Figs. 6 and 7 show the O-ring gap changes as a function of the clearance δ_4 for the case when the primary O-ring seals the joint and for the case when the secondary O-ring seals the joint. A band of results that corresponds to clearances ranging from $\delta_1 = \delta_2 = 0$ to 0.127 cm (0.050 in.) and that includes all combinations of clearances in between these bounding values is shown in Figs. 6 and 7. Results were obtained for values of $\delta_3 = 0$ and 0.127 cm (0.050 in.) that indicated no significant effect of varying δ_3. Results for the original joint (independent of δ_4) are overlayed in Figs. 6 and 7 to highlight the advantage of the redesigned joint.

Another important parameter appearing in Figs. 6 and 7 is the clearance μ. This clearance is defined as the mismatch in the width of the channel that the clevis inner leg slides into (dimension t_1 in the figures) and the width of the clevis inner leg (dimension t_2 in the figures). Moreover, the clearance μ is also the sum of the clearances δ_4 and δ_5 as indicated in Fig. 3b. A zero value of μ implies a perfect metal-to-metal assembly of the clevis inner leg and the capture feature with no clearance on either side of the clevis inner leg. This type of assembly would be very difficult to perform without damaging the O-rings in the joint, and results for this parameter are included herein to give an indication of the effect of reducing μ. The

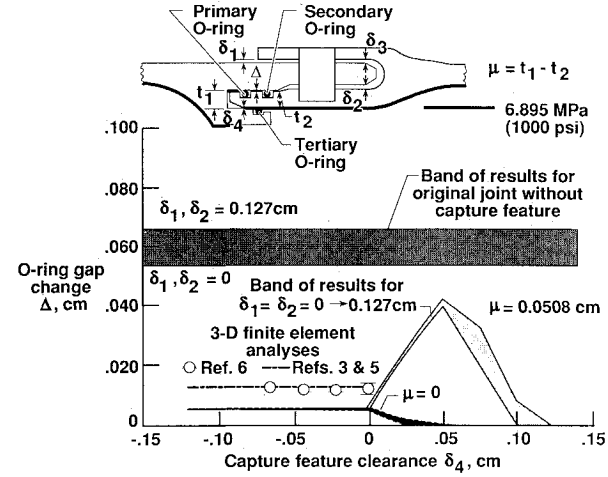

Fig. 6 Effect of clearances on O-ring gap changes of redesigned joint. Pressure seal at primary O-ring.

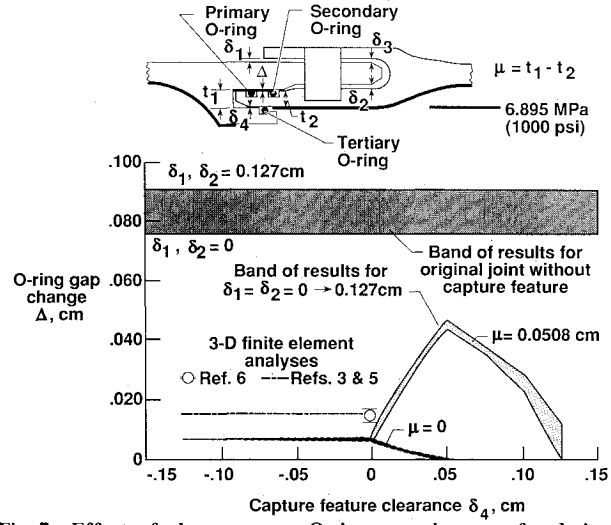

Fig. 7 Effect of clearances on O-ring gap changes of redesigned joint. Pressure seal at secondary O-ring.

nominal value of μ that is considered to be representative of the actual flight hardware assembly is taken to be 0.051 cm (0.020 in.) in the present study.

The most important parameter used in the design of this joint, and appearing in these figures, is the clearance δ_4. Positive values of δ_4 correspond to a relative positioning of the capture feature and clevis inner leg, prior to assembly, such as that depicted in Fig. 8a. In this case, no contact is made between the outer surface of the capture feature (surface facing the outside of the shell) and the inner surface of the clevis inner leg when the joint is assembled (see Fig. 8b). For joints with $0 < \delta_4 \leq \mu$, the relative positioning of the tang and clevis inner leg results in no contact between the clevis inner leg and either the capture feature or the tang when the joint is assembled. In this case, the joint exhibits the largest O-ring gap changes, and behaves in a manner similar to that of the original joint; i.e., the O-ring gap changes are determined by the relative stiffnesses of the tang and clevis and are not influenced by any preloading due to an interference fit assembly. For joints with large values of δ_4 (greater than μ), the relative positioning of the tang and clevis inner leg causes contact between the inner surface of the tang and the outer surface of the clevis inner leg when the joint is assembled. After assembly, the clevis inner leg and tang are deformed so that they tend to remain in contact when subjected to motor pressurization. This behavior is manifested in Figs. 6 and 7 by the reduction in the O-ring gap change as δ_4 becomes greater than μ. The increased force holding the clevis inner leg against the tang, associated with the

increase in δ_4, causes the reduction in the size of the O-ring gap changes. However, as δ_4 increases beyond μ, the likelihood of damaging the primary and secondary O-rings during joint assembly also increases, and is thus undesirable since these O-rings constitute the primary sealing mechanism of the joint.

Negative values of δ_4, referred to herein as an interference fit, correspond to a relative positioning of the capture feature and clevis inner leg, prior to assembly, such as that shown in Fig. 9a. With an interference fit, the tertiary O-ring in the capture feature is locked against the inner surface of the clevis inner leg and does not move during motor pressurization. However, because of the possibility of damage during motor assembly, associated with an interference fit, the tertiary O-ring seal is not relied on as a primary sealing mechanism in the redesigned joint. After joint assembly, the capture feature and the clevis inner leg are deformed so that they will remain in contact when the joint is pressurized, as indicated in Fig. 9b. The results in Figs. 6 and 7 indicate that this deformed state has the positive effect of allowing only very small O-ring gap changes when the joint becomes pressurized, as indicated in Fig. 9c.

Results of similar parametric studies of the redesigned joint involving substantially fewer joint parameters and obtained using three-dimensional finite-element analyses are presented in Refs. 3, 5, and 6. More specifically, results showing the effects of the clearance δ_1 associated with the prelaunch shimming process, the capture feature clearance δ_4, and the pressure seal location on the O-ring gap changes are presented in Refs. 3, 5, and 6. The elastic analyses presented in these references (for these three parameters mentioned previously) indicate good qualitative agreement with the corresponding results presented herein and suggest that the FASOR analysis adequately captures the qualitative behavior of the joint. Typically, the results obtained from three-dimensional finite-element analyses yielded somewhat larger O-ring gap changes than the results obtained from the FASOR analyses, but both analyses indicated the same trends. The larger gap changes obtained from the finite-element analyses are attributed to the more accurate three-dimensional flexibility of the finite-element models and the inclusion of clearances around the pin connection that are not included in the shell analysis presented in this paper. The pertinent results presented in Refs. 3, 5, and 6 are reproduced in Figs. 6 and 7.

The results of the present study presented in Figs. 6 and 7 indicate that the redesigned joint has essentially the same behavior for the two pressure seal cases with O-ring gap changes of the same size [<0.051 cm (0.020 in.)] that are substantially smaller than those of the original joint. In addition, the results of the present study shown in Figs. 6 and 7 indicate that the interference fit (given by negative values of δ_4) yields substantially smaller O-ring gap changes in most cases than the fit with large positive values of δ_4 and exhibits much less sensitivity to variations in the clearances δ_1 and δ_2. The results of three-dimensional finite-element analyses presented in Refs. 3, 5, and 6, and shown in Figs. 6 and 7, also indicate O-ring gap changes substantially smaller than those of the original joint when an interference fit is used. Both the results of the present study and the three-dimensional finite-element results indicate that the size of the O-ring gap change is essentially independent of the amount of interference between the capture feature and the clevis inner leg for both pressure seal cases. O-ring gap changes of 0.0132 cm (0.0052 in.) and 0.0158 cm (0.0062 in.) for an interference fit and pressure seals at the primary and secondary O-rings, respectively, are reported in Refs. 3 and 5. These results correspond to clearances on the order of $\mu = 0.025$ cm (0.010 in.) and $\delta_1 = 0.018$ cm (0.007 in.). Values of O-ring gap changes ranging between 0.0109–0.0147 cm (0.0043–0.0058 in.) corresponding to various interference fits with $\mu = 0.023$ cm (0.009 in.), δ_1 on the order of 0.025 cm (0.010 in.), and with a pressure seal at the primary O-ring are reported in Ref. 6 (see Fig. 6). The results presented in Ref. 6 also indicate a slight sensitivity of the O-ring gap changes to the clearance δ_1 for the case of $\delta_4 = 0$ ($\mu = 0.023$ cm). The results are shown in Figs. 6 and 7 for $\delta_4 = 0$ and correspond to δ_1 varying between 0 and ~ 0.076 cm (0.030 in.).

The results of the present study presented in Figs. 6 and 7 also indicate that reducing the clearance μ results in only slight reductions in the size of the O-ring gap changes for joints with an interference fit. In contrast, the results presented in Figs. 6 and 7 indicate that reducing the clearance μ results in substantially reducing the O-ring gap changes and sensitivity to clearances for joints having positive values of clearance δ_4. However, it should be reiterated that reducing the clearance μ increases the possibility of damaging the O-rings during motor assembly and losing the pressure seal altogether. The results presented in Figs. 6 and 7 indicate that an interference fit is practically insensitive to the clearance μ in addition to yielding small O-ring gap changes, and is thus an attractive joint design.

An important result depicted in Figs. 6 and 7 is the indication that, due to the presence of the capture feature, the redesigned joint behaves essentially the same whether the primary or secondary O-ring provides the pressure seal. This result is substantiated by both the shell analyses presented herein and the three-dimensional finite-element analyses presented in Refs. 3, 5, and 6. This similar behavior means that if the primary O-ring fails to seal the joint then the secondary O-ring only has to undergo modest displacements of the same order to reseal the joint. This attribute of the redesigned joint, particularly with an interference fit, is a significant improvement over the original joint (see Fig. 5) in which the size of the

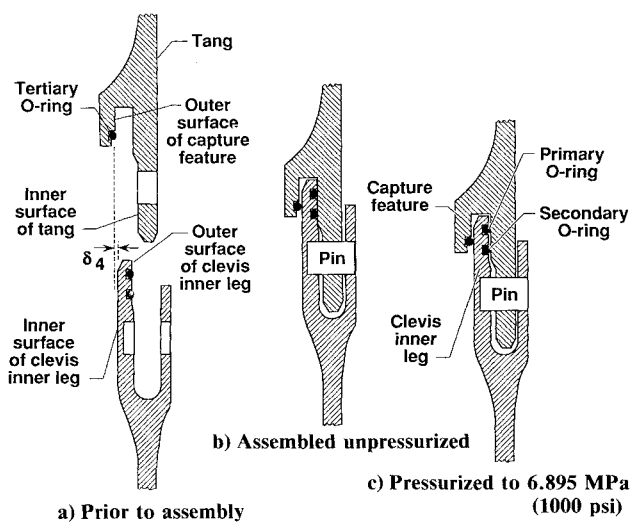

Fig. 8 Capture feature clearances of redesigned joint ($\delta_4 > 0$).

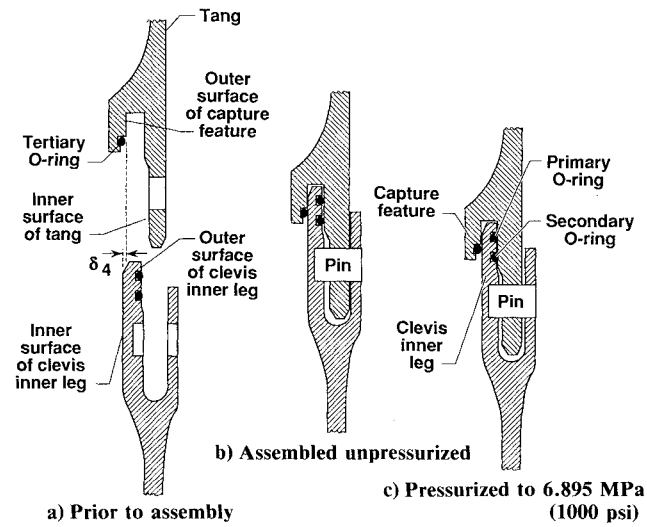

Fig. 9 Capture feature clearances of redesigned joint ($\delta_4 < 0$).

O-ring gap change increases by about 45% when the pressure seal moves from the primary O-ring to the secondary O-ring. The results presented in Figs. 6 and 7 suggest another significant point. Specifically, the motor cases are 3.7 m (12 ft) in diameter and are not perfectly circular to within very small tolerances. Thus, after assembly, the actual flight article may be operating over the entire spectrum of the results presented in these figures for various circumferential locations.

Concluding Remarks

Results of axisymmetric shell analyses have been presented for the original and redesigned Space Shuttle solid rocket booster field joints. The results were obtained using the shell-of-revolution computer code known as FASOR. Details of the modeling issues, a generic method for simulating contact in the joint, and the way in which the shell analysis treats these modeling issues have been discussed. Results of an in-depth parametric study of the structural behavior of the joints as a function of initial clearances have been presented. Comparisons of the axisymmetric shell analyses with experimental results obtained by Morton Thiokol and with three-dimensional finite-element analyses have also been presented for a few joint parameters. These comparisons indicate that the results of the shell analyses agree well qualitatively with the experimental results and the results of the three-dimensional finite-element analyses, and can be used to identify the structural response trends and to serve as a guide for more detailed three-dimensional finite-element analyses.

A wide range of parametric results for the original joint indicate how the radial distance (referred to herein as O-ring gap change) separating adjacent surfaces of the tang and clevis inner leg between the primary and secondary O-rings changes as a function of initial clearances, pressure seal location, and geometric nonlinearity have been presented. These results indicate that substantial increases in the O-ring gap changes occur (about 45%) when the primary O-ring fails and the secondary O-ring then seals the joint. These results also indicate a moderate sensitivity of the O-ring gap changes to initial joint clearances and a benign effect of geometric nonlinearity.

A wide range of parametric results have also been presented for the redesigned joint that indicate its behavior as a function of initial clearances and pressure seal location. These results indicate that the addition of the capture feature to the redesigned joint significantly reduces the size of the O-ring gap changes and the sensitivity to joint clearances compared to the original joint. In addition, the results show that the redesigned joint exhibits practically the same size O-ring gap changes and behavior trends regardless of whether the primary or secondary O-ring seals the joint, unlike the original joint. Furthermore, the results indicate that the interference fit configuration provides a good pressure seal.

Appendix: Contact Modeling Details

The basic FASOR models of the original and redesigned SRM joints do not account for contact between adjacent shell segments during structural deformation. Specifically, adjacent shell segments are free to overrun one another for certain loadings and initial clearances. To rectify this deficiency in the basic shell analysis, an influence coefficient method is used in conjunction with the FASOR models to obtain contact forces that prevent overrun of adjacent shell segments and that hence provide more accurate physical models of the SRM joints. The general contact simulation procedure is identical for the original and redesigned joints, and is illustrated in this section only for the redesigned joint.

The influence coefficient method presented herein is based on applying pairs of self-equilibrating loads, referred to hereafter as influence loads, to points on adjacent shell segments that could come into contact with one another during deformation. There are assumed to be seven locations involving 11 points on the shell where contact could occur with associated contact forces F_1 through F_7 as indicated in Fig. A1. Pairs of influence loads are applied in separate FASOR runs to determine the influence coefficients Δ_{rj}, which are defined as the deflection of point r due to the influence loading associated with F_j. The influence loads are inversely proportional to the radii of adjacent shell walls in order to satisfy force equilibrium of adjacent differential elements of the two shell walls. Influence coefficients Δ_{rp} are also determined for a unit pressure loading on the shell. If δ_j is the initial gap between adjacent shell wall surfaces (radial distance between adjacent shell wall surfaces before assembly and loading), the final gap G_j after assembly and loading is given by

$$G_j = P(\Delta_{rp} - \Delta_{sp}) + \sum_{i=1}^{N} F_i(\Delta_{ri} - \Delta_{si}) + \delta_j \qquad \text{(A1)}$$

where the subscript j ranges from 1 to N, the number of contact locations. The subscripts r and s represent two adjacent contact points associated with the contact forces F_j shown in Fig. A1. The multiplier P is used to specify the intensity of the actual pressure loading under consideration. Setting $P = 0$ corresponds to the case of contact forces produced by joint assembly. Because of the close proximity of certain locations, the number of clearance parameters used in the study was reduced by requiring that $\delta_6 = \delta_4$ and $\delta_7 = \delta_5$. In addition, the parameters δ_4 and δ_5 should not be considered completely independent. The parameter $\mu = \delta_4 + \delta_5$ has been introduced to better reflect the possible geometry of the joint. Positive values of μ indicate clearance between capture feature and clevis inner leg, whereas negative values indicate that the clevis inner leg is larger than the channel formed by the capture feature that it slides into.

Setting all of the gaps G_j equal to zero and solving Eq. (A1) for F_i gives the contact forces at all of the assumed contact points. In general, however, some of the contact forces will be negative indicating that a tensile force is required for displacement compatibility. This solution is not physically admissible. A physically admissible solution to Eq. (A1) is one in which all of the contact forces F_j are either positive or zero, and the gaps G_j are zero for the locations with positive F_j and positive for the locations with zero F_j. A negative value of G_j indicates that two adjacent surfaces have overrun each other and is inadmissible. Computationally, this process corresponds to eliminating the equations and contact forces associated with points not in contact from Eq. (A1). This elimination step is performed by using the information about points not in contact to define a pivotal strategy in a Gaussian elimination subroutine.

The unique contact solution may be found by considering all possible combinations for $F_j = 0$ in Eq. (A1), solving the reduced set of equations obtained by including only those with nonzero F_j, and then calculating G_j for the locations having $F_j = 0$. If N is the number of pairs of possible contact points,

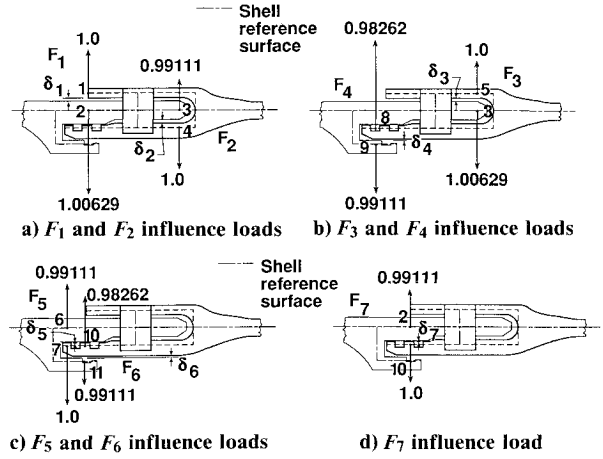

a) F_1 and F_2 influence loads b) F_3 and F_4 influence loads

c) F_5 and F_6 influence loads d) F_7 influence load

Fig. A1 Clearances, nondimensional influence loads, and contact points of redesigned joint.

which may be either open or closed, there are 2^N total number of contact combinations that must be considered. The analysis of all the various load combinations is facilitated by considering the 2^N binary numbers from 0 to 2^N-1. Each digit in the binary number is assigned to one of the locations and the load at that location is taken to be zero or nonzero according to whether there is a 0 or 1 in that particular digit of the binary number. For seven possible contact locations ($N=7$), there are 128 combinations that need to be considered; i.e., 1 combination taking 7 F_j at a time, 7 combinations taking 6 F_j at a time, 21 combinations taking 5 F_j at a time, 35 combinations taking 4 F_j at a time, 35 combinations taking 3 F_j at a time, 21 combinations taking 2 F_j at a time, 7 combinations taking 1 F_j at a time, and 1 combination taking 0 F_j at a time (no contact). Because this is a physical problem that has a unique solution, only one of these combinations will satisfy all of the required conditions. Solutions for the original SRM joint are obtained by considering only the three equations of Eq. (A1) corresponding to F_1, F_2, and F_3. All 7 F_j are considered for the redesigned joint.

Solution Procedure for Nonlinear Analysis

The nonlinear solutions for the original and redesigned joints were obtained using the contact formulation previously described. First, a linear solution is obtained from which the values and locations of the nonzero contact forces are obtained. The nonzero contact forces are then applied to the FASOR model in addition to the motor pressure loading, and a nonlinear analysis is performed. From the nonlinear analysis a new set of displacements $\tilde{\Delta}_{rp}$ and $\tilde{\Delta}_{sp}$ are obtained. The displacements $\tilde{\Delta}_{rp}$ and $\tilde{\Delta}_{sp}$ are then substituted into Eq. (A1), replacing $\tilde{\Delta}_{rp}$ and $\tilde{\Delta}_{sp}$, and increments to the contact forces are obtained by solving Eq. (A1). The increments to the contact forces are for the same contact combination produced by the linear solution and do not account for any change in the contact location. Following this procedure, the increments to the contact forces obtained from the solution of Eq. (A1) may be positive, negative, or zero. This process is repeated until the increments for the contact forces are negligible compared to their total values.

References

[1]*Report of the Presidential Commission on the Space Shuttle Challenger Accident,* Washington, DC, June 6, 1986.

[2]Cohen, G. A., FASOR—*Field Analysis of Shells of Revolution User Manual*, Structures Research Associates, Laguna Beach, CA, Rev. T, March 14, 1986.

[3]Greene, W. H., Knight, N. F., Jr., and Stockwell, A. E., "Structural Behavior of the Space Shuttle SRM Tang-Clevis Joint," *Journal of Propulsion and Power,* Vol. 4, No. 4, 1988.

[4]Oostyen, J. E., Bright, D. D., Hawkins, G. F., McCluskey, P. M., and Larsen, G. L., *SRM Joint Deflection Referee Tests: Phase 2 Final Report,* Wasatch Operations, Morton-Thiokol, Inc., Brigham City, UT, Doc. TWR-300149, April 3, 1986.

[5]Card, M. F. and Wingate, R. T., "Structural Behavior of Solid Rocket Motor Field Joints," *Proceedings of the AIAA/ASME/ASCE/AHS 28th Structures, Structural Dynamics, and Materials Conference,* AIAA, New York, 1987.

[6]Hill, M. L., Coulter, J. C., Matharu, S. S., and Whelchel, T. M., *Solid Rocket Motor: Critical Design Review (CDR) Structural Analysis of the Solid Rocket Motor Redesigned Field Joint,* NASA Marshall Space Flight Center, MSFC-RPT-1474, Dec. 1987.

ATTENTION JOURNAL AUTHORS:
SEND US YOUR MANUSCRIPT DISK

AIAA now has equipment that can convert virtually any disk (3½-, 5¼-, or 8-inch) directly to type, thus avoiding rekeyboarding and subsequent introduction of errors. The mathematics will be typeset in the traditional manner, but with your cooperation we can convert text.

You can help us in the following way. If your manuscript was prepared with a word-processing program, please *retain the disk* until the review process has been completed and final revisions have been incorporated in your paper. Then send the Associate Editor *all* of the following:

- Your final version of double-spaced hard copy.
- Original artwork.
- A *copy* of the revised disk (with software identified).

Retain the original disk.

If your revised paper is accepted for publication, the Associate Editor will send the entire package just described to the AIAA Editorial Department for copy editing and typesetting.

Please note that your paper may be typeset in the traditional manner if problems arise during the conversion. A problem may be caused, for instance, by using a "program within a program" (e.g., special mathematical enhancements to word-processing programs). That potential problem may be avoided if you specifically identify the enhancement and the word-processing program.

In any case you will, as always, receive galley proofs before publication. They will reflect all copy and style changes made by the Editorial Department.

If you have any questions or need further information on disk conversion, please telephone Richard Gaskin, AIAA Production Manager, at (202) 646-7496.